PAPER

Check for updates

Mid-infrared GaAs/AlGaAs micro-ring resonators characterized *via* thermal tuning

Julian Haas, [ID] Philipp Artmann and Boris Mizaikoff [ID] *

Micro-ring resonators with a decoupling waveguide have been manufactured from GaAs/Al$_{0.2}$Ga$_{0.8}$As, accommodating mid-infrared wavelengths, and were characterized *via* thermal tuning. A *Q*-factor of 1900, a thermal full width at half maximum of 8 °C, and a thermal free spectral range of 18 °C have been achieved. The low *Q*-factor indicates comparatively high coupling efficiency from the input waveguide into the decoupling waveguide. The micro-ring resonators shown herein are suitable structures for advanced mid-infrared chem/bio sensing strategies *via* resonant-cavity enhancement. In addition, they offer high spectral resolution for evanescent field sensing strategies *via* effective wavelength de-multiplexing waveguide structures.

Introduction

Optic circuitry in the visible spectral regime enabling, *e.g.*, integrated on-chip sensing applications is dominated by silicon and related silicon-on-insulator (SOI) CMOS compatible designs.[1–3] A wide variety of logical gates and de-multiplexing elements such as single beam splitters, multiple beam splitters, and Mach–Zehnder interferometer (MZI) structures are deployed for, *e.g.* wavelength de-multiplexing. Micro-ring resonators are straight forward optical structures, enabling decoupling of radiation at a precisely defined wavelength, either determined by the ring dimensions[4] or controlled *via* precise refractive index tuning, *e.g.*, *via* thermal tuning strategies.[5,6] For this task, different geometries, comprising micro-toroids,[7–9] whispering galley mode resonators (*e.g.*, micro-disks), and designs with elongated coupling regions such as race-track, sling or pulley couplers have demonstrated effective operation.

However, such devices are virtually exclusively tailored for and limited to telecom wavelengths, *i.e.*, the near infrared (NIR) around 1.3–1.6 μm. Besides applications in telecommunications technology, chemical sensing *via* more or less sophisticated optical transducers has increasingly matured during recent years, frequently taking advantage of such structures for various sensing tasks.[10,11] For example, Lechuga *et al.* have shown applications of MZI and bimodal waveguides for the detection of biomolecules.[12,13] Also, micro-toroids have been integrated into chemical sensing tasks,[14] likewise, the detection of nanoparticle aggregation has been shown for slotted ring resonators.[15] Crespi *et al.* have shown applications utilizing more sophisticated quantum states of light, thereby harnessing sophisticated optical structures for protein sensing. However,

extending chem/bio sensing schemes from the visible and NIR into the mid-infrared (MIR; 3–12 μm) spectral region has to date been limited by appropriate materials that are transparent in this spectral window.[16–19] Chem/bio sensing *via* the evanescent field emanating from the waveguide structure especially benefits from extending the wavelength of the utilized radiation into the MIR. Since the penetration depth of the evanescent field into an adjacent analyte matrix directly depends on the wavelength of the utilized radiation, the evanescent field in the MIR extends up to several μm away from the waveguide surface. In comparison to visible and NIR frequencies, an increased analyte volume is probed, which enables detecting minute analyte quantities at improved limits of detection.

Recently, a silicon-on-sapphire (SOS) ring resonator concept has been shown operating at wavelengths ranging from 2.75 μm (ref. 20 and 21) to 5.5 μm (ref. 22) and 8 μm.[23] Chalcogenide glass waveguides have been presented for operation around 5.2 μm (ref. 24) and germanium-based strategies have been presented for operation in the long wave mid infrared.[25,26]

As an alternative, the III–V semiconductor material gallium arsenide (GaAs) may be deposited onto an optical buffer layer made from aluminium gallium arsenide (AlGaAs) thus providing a possibly wide transparent window in the MIR (*i.e.*, 0.9–25 μm), as pioneered by Mizaikoff and collaborators.[27,28] GaAs/AlGaAs systems therefore can be utilized throughout the whole near-, mid- and far-infrared with the possibility to monolithically integrate the waveguides with sources, especially quantum cascade lasers (QCLs), and detector schemes. What is more, AlGaAs represents a readily available buffer layer as the design for adequate lower refractive index cladding layers can be challenging for chalcogenide classes. A variety of applications using slab and ridge waveguides, as well as a thin-film MIR-MZI designs have been demonstrated and applied in exemplary chem/bio sensing scenarios.[29–32] Based on design

Institute of Analytical and Bioanalytical Chemistry, Ulm University, Albert-Einstein-Allee 11, D-89081 Ulm, Germany. E-mail: boris.mizaikoff@uni-ulm.de

studies by Sieger *et al.*,[33] GaAs/AlGaAs MIR thin-film waveguide structures may readily be designed and optimized for single-mode propagation.

Experimental

Simulation

The micro-ring resonators presented in this study were optimized for a resonance frequency around 6 μm.

In this spectral region, various biologically relevant analytes such as proteins are characterized by pronounced and molecularly selective absorption features. Hence, cavity-enhanced sensing schemes, enabling ultra-sensitive analysis or high-resolution wavelength splitting, facilitating advanced absorption spectroscopy based chem/bio sensing schemes may be realized *via* the presented structures, and may be extended into the fingerprint spectral regime (>10 μm) for other analytes in the future. Theoretical modelling of wavelength dependent transmission properties of the presented resonator structures was merged with temperature dependent transmission spectra of waveguide structures that were subsequently manufactured according to the developed design input.

The basic design parameters (free spectral range, FSR; full width at half maximum, FWHM) of optical micro-ring resonators derive as shown in eqn (1) and (2)

$$FSR = \Delta\lambda = \frac{\lambda^2}{n_{eff} L_{ring}} \tag{1}$$

$$FWHM = 2\delta\lambda = \frac{\lambda^2}{\pi L n_{eff}} \frac{1 - t^2}{t} = \frac{\kappa^2 \lambda^2}{\pi L_{ring} n_{eff}} \tag{2}$$

with the effective refractive index n_{eff}, the resonator length L_{ring}, the utilized wavelength λ, and the coupling efficiency parameters t and κ, whereby $|t|^2 + |\kappa|^2 = 1$. Consequently, for a resonator length of 1560 μm, an effective refractive index of 3.24 and a value for t of 0.9, a FSR of 7 nm, and a FWHM of 0.48 nm can be calculated at a wavelength of 6 μm. Furthermore, a quality factor (Q-factor) of the micro-ring resonator of 12 500 can be derived using eqn (3)

$$Q = \frac{\lambda}{FWHM} \tag{3}$$

For a more precise approximation of the expectable resonance behaviour, finite element method (FEM) calculations were performed using COMSOL Multiphysics considering a waveguide thickness of 6 μm and a coupling trench width of 200 nm. A wavelength resolution of $\Delta\lambda = 33$ pm was selected to accurately model and resolve the expected spectral features (Fig. 1). For a ring resonator without an additional decoupling port, a FWHM of 0.45 nm or 0.12 cm^{-1}, respectively, was calculated, which translates into a theoretical Q-factor of approx. 13 000 at a centre wavelength of 5.99 μm. For a ring resonator with an additional decoupling port, a FWHM of 0.23 nm or 0.07 cm^{-1}, respectively, was calculated, which gives rise to a theoretical Q-factor of approx. 25 000 at a centre wavelength of 5.96 μm. Furthermore, the transmission intensity
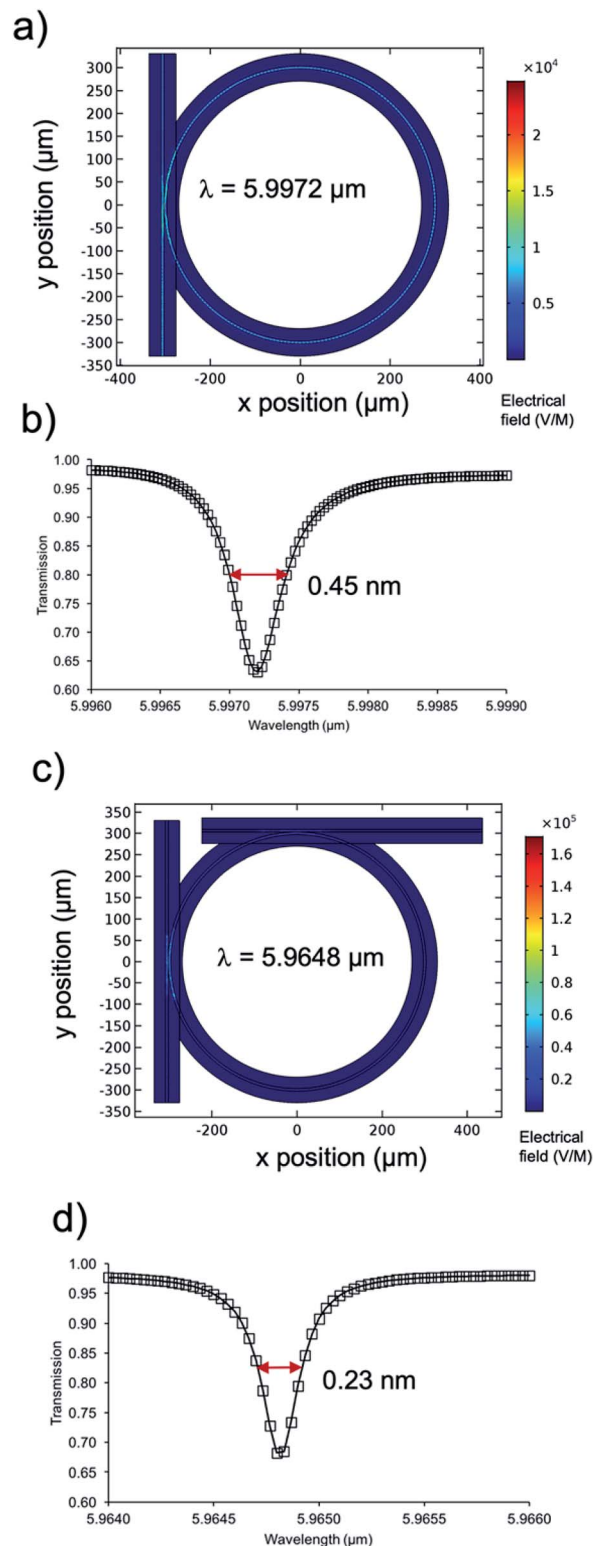

Fig. 1 (a) 2D FEM simulation of a 6 μm GaAs micro-ring resonator showing the electrical field intensity. (b) Resonance dip for the plotted transmission of the throughput port of the structure shown in (a). (c) FEM simulated electrical field intensity for a micro-ring resonator with an out-coupling port. (d) Corresponding resonance dip at the throughput port of the structure shown in (c).

at the resonance frequency is reduced by approx. 32% in both cases. Due to the idealized model, the all-pass resonator without any de-coupling port represents an over-coupled resonator in which excess energy is coupled back from the ring into the waveguide (Fig. 1(a) and (b)). As a result, fewer round-trips are possible and a broader bandwidth is coupled into the ring, leading to a broader FWHM and a lower Q-factor in comparison to the micro-ring resonator with an out-coupling port. The additional out-coupling port (add-drop configuration) reduces back-coupling into the in-coupling port and thus leads to a narrower FWHM of the resonance dip and a higher Q-factor, respectively (Fig. 1(c) and (d)). The derived values for the FWHM and Q-factors are well in agreement with the values calculated *via* eqn (1) and (2), which confirms that these models are valid for the waveguide structures designed herein.

Waveguide fabrication

GaAs waveguide structures with a thickness of 6 μm were epitaxially grown onto a 6 μm buffer layer of $Al_{0.2}Ga_{0.8}As$, which was deposited onto a heavily n-doped GaAs substrate wafer.

The waveguides structures were patterned *via* photolithography and *via* reactive ion etching (RIE) using $SiCl_4$/Ar dry chemistry. In brief, the photoresist (AZ ECI 3027, Allresist GmbH, Strausberg, Germany) was spin-coated onto the wafer, exposed *via* a manual mask aligner (SUSS-MJB3, Suss Microtec GmbH, Garching, Germany), and developed in a puddle (AZ MIF 726, Allresist GmbH, Strausberg, Germany) for defining the waveguide structures *via* the photoresist. Final waveguide patterning was achieved *via* reactive ion etching (RIE) using $SiCl_4$/Ar dry chemistry (10 sccm/6 sccm, 35 W RF, $p = 15$ mTorr, Plasmalab System 100, Oxford Plasmalab, Yatton, UK). The precise definition of the coupling trench was achieved *via* focused ion beam (FIB) milling (Quanta 3D FEG, FEI Eindhoven, Netherlands). After fabrication of the waveguides, the coupling facets were cleaved using a diamond knife facilitating effective in-coupling from free space.

Finally obtained waveguides comprised a tapered in-coupling region, a straight section with the ring-resonator, and a straight out-coupling waveguide oriented perpendicular to the in-coupling waveguide structure.

Fig. 2 gives an example of a GaAs micro-ring resonator (6 μm wide, 6 μm high) with a diameter of approx. 496 μm, and a length of approx. 1450 μm along with alignment waveguides, in-coupling waveguide, and de-coupling waveguide (a). Fig. 2(b) shows the front view of a cleaved GaAs waveguide facet (6 × 6 μm) deposited onto an $Al_{0.2}Ga_{0.8}As$ buffer layer (thickness 6 μm) revealing a neat end facet with minimal scattering losses.

Furthermore, the substrate was heavily n-doped ensuring its opaqueness in the MIR, and thus, reducing light scattering or coupling into the substrate. Fig. 2(c) reveals a close-up view of a FIB-milled coupling trench with a spacing of approx. 200 nm. However, due to re-deposition during the FIB-milling process slightly V-shaped sidewalls are to be expected. Hence, the formation of waveguide ribs is likely. Fig. 2(d) shows a complementary FEM simulation of the confined electrical field at a wavelength of 6 μm within a 6 × 6 μm GaAs waveguide
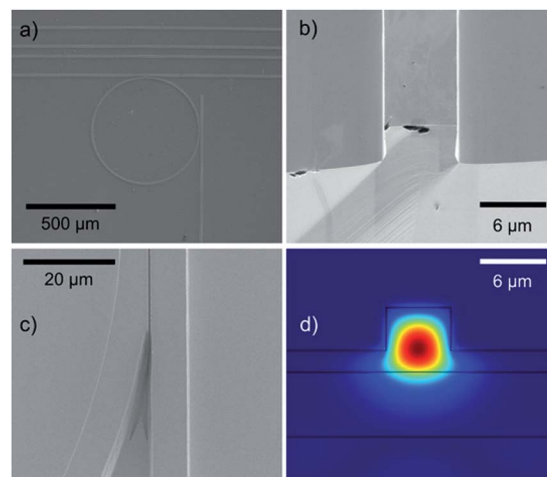

Fig. 2 (a) Example of a GaAs micro-ring resonator along with alignment waveguides, as well as in-coupling and de-coupling waveguides. (b) Skewed top and front view of an end-facet and the top side of a tilted GaAs waveguide (6 μm × 6 μm) deposited onto an $Al_{0.2}Ga_{0.8}As$ buffer layer (6 μm). (c) Magnified view of a FIB-milled coupling trench with a spacing of approx. 200 nm. (d) FEM simulation of the confined electrical field ($\lambda = 6$ μm) within a 6 μm × 6 μm GaAs waveguide modelled on top of an $Al_{0.2}Ga_{0.8}As$ buffer layer, which forms a rib due to potential incomplete etching of the GaAs layer within coupling trenches.

modelled on top of a $Al_{0.2}Ga_{0.8}As$ buffer layer, which forms a 2 μm rib waveguide due to incomplete etching of the GaAs layer. The calculated pronounced confinement of the electrical field within the 6 μm structure ensures that evanescent field coupling to the resonator is enabled.

Waveguide characterization

Linear polarized (100 : 1) radiation was provided by a broadly tuneable external cavity quantum cascade laser (EC-QCL, Mircat 1000-7603, Daylight Solutions Inc., San Diego, USA) operated in continuous wave (cw) mode with a typical, manufacturer given, linewidth of <0.003 cm^{-1} or about 0.01 nm at a wavelength of 6 μm, respectively. Emanating radiation at the distal end of the waveguide structure was detected *via* a liquid nitrogen cooled (LN_2) mercury-cadmium-telluride (MCT) semiconductor detector (Kolmar Technologies Inc., Newburyport, USA).

Thermal tuning was performed *via* an external resistive heating device (Watlow EZ-Zone, Watlow GmbH, Kronau, Germany). The temperature was monitored using a type K NiCrNi thermocouple. Both, intensity and temperature data were recorded *via* an AD converter (NI USB-9162 National Instruments GmbH, München, Germany), and a custom control software programmed in Labview (Labview 2014, SP1, V 14.0f3, National instruments GmbH, München, Germany). A schematic layout of the experimental setup is shown in Fig. 3.

Results & discussion

Since the calculated narrow resonance dips of micro-ring resonators impose highly precise tuning and high wavelength resolution on the QCL, temperature tuning has been introduced
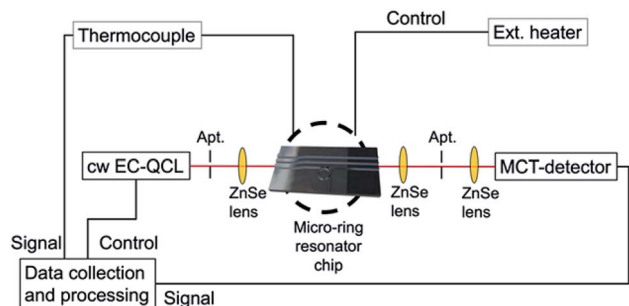
Fig. 3 Scheme of the experimental setup comprising a cw EC-QCL, a MCT-detector, an external heating system, and a thermocouple. Incident radiation is shaped *via* apertures and focused onto the waveguide facet using zinc selenide (ZnSe) lenses. Micro-ring resonator chip, electrical heater, and the thermocouple are in thermal contact.

by Tsang *et al.*[21] as powerful strategy for estimating micro-ring resonator characteristics at single wavelength emission *via* precise temperature tuning of the resonant cavity. While this was readily achieved using conventional temperature controller units, propagation losses and temperature dependency of the coupling efficiency between the waveguides and the ring structure were assumed to be temperature independent in the evaluated temperature range in this simplified model. Furthermore, the linear coefficient of thermal expansion of GaAs is in the order of 10^{-6} K^{-1},[34] which is two orders of magnitude lower than the thermo-optic coefficient of GaAs and therefore neglectable in the performed analysis. Moreover, thermo-optic effects of AlGaAs are assumed to be negligible (*i.e.*, thermo-optic effect of GaAs of $\partial n/\partial T = 2.35 \times 10^{-4}$ (ref. 35)). In analogy to wavelength tuning, the determination of a Q-factor *via* eqn (4) has been derived as

$$Q = \frac{\lambda_{\mathrm{m}}}{\delta\lambda_{\mathrm{O}}} \cong \frac{\Delta T}{\delta T} \frac{n_{\mathrm{eff}} L_{\mathrm{ring}}}{\lambda_{\mathrm{m}}} \qquad (4)$$

with the resonances in the temperature domain ΔT at the same wavelength λ_{O} and the thermal FWHM δT. Furthermore, $\Delta T/\delta T$ is considered equal to the finesse F of the resonator. Prior to thermal tuning, loss of the waveguide was determined at room temperature at 5.5 μm. A comparably high loss of 18 dB cm^{-1}, ε = 4.3 cm^{-1} respectively, indicates loss paths, that are not alone material inherent. Coupling losses, due to the diffraction limited diameter of the spot size of the focused beam of about 20 μm and potential back reflection are more likely to superimpose the material inherent losses. Since the system loss was determined by comparing the incident energy before incoupling with the transmitted energy after decoupling, bulk losses were determined including any insertion losses. However, determining bulk losses of the on-chip waveguides together with the focusing optics yields a realistic estimation of the expected practical losses. Evaluation and optimization of coupling motives and microscopic scattering paths, *e.g.* at the waveguide sidewalls will be pursued during future studies. The transmission of the throughput port was experimentally determined in a temperature range of 35 to 80 °C. As a reference, the transmission behaviour of straight waveguides was evaluated to

separate non-ring-related deviations from the ideal transmission characteristics, as required for eqn (4) to be applicable, which may arise from end-facet fringing or thermally induced coupling of noise (Fig. 4(a)). Transmission curves for thermal tuning of the micro-ring resonator structures were recorded at wavelengths of 5.5 μm, 5.6 μm, 5.7 μm, 5.8 μm, and 5.9 μm. From the thermal tuning emission curves (two curves are exemplarily shown in Fig. 4(b)), values for $\Delta T = (18 \pm 2)$ °C and $\delta T = (8 \pm 1)$ °C were derived. Consequently, a Q-factor of about 1900 was calculated along with a finesse of 2.25.

Furthermore, a roundtrip loss factor of $\alpha = 0.4 \pm 0.1$, and a field coupling coefficient of $t = 0.6 \pm 0.2$ was derived. However, the temperature tuning curves are superimposed by arbitrary spikes of the detected intensity that can be assigned to mode-hops and emission instabilities of the QCL resulting from random fluctuations in laser chip temperature and applied current appearing randomly during cw operation at a fixed wavelength (*i.e.* at non-stabilized operation conditions). Apart
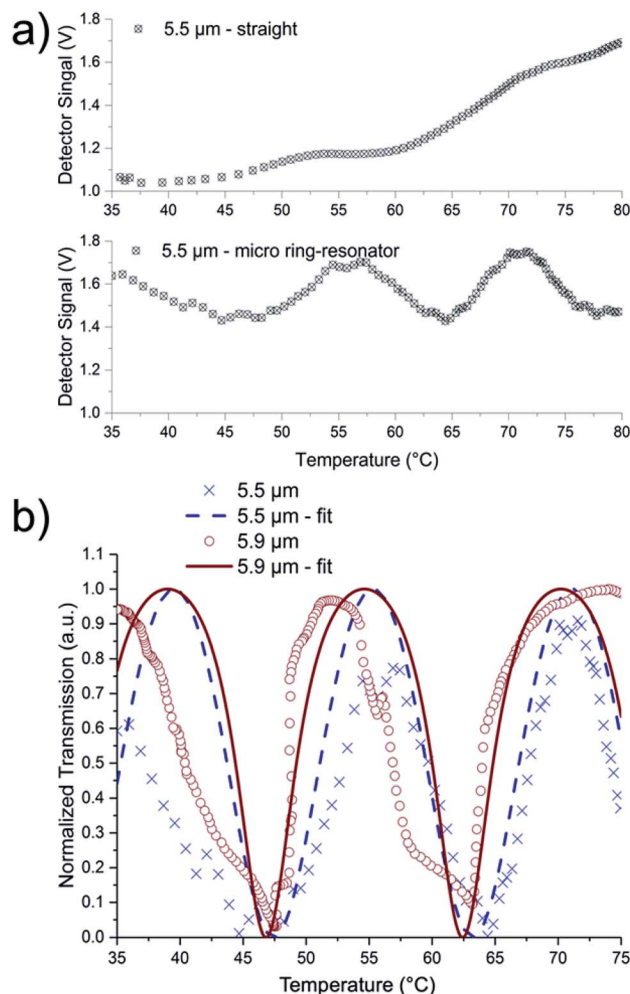

Fig. 4 (a) Transmission behaviour of a straight waveguide only without pronounced dips *vs.* a waveguide with a coupled micro-ring resonator. (b) Resonance behaviour during thermal tuning exemplarily shown at two selected wavelengths, corrected by the transmission behaviour of a straight waveguide at the respective wavelength to correct for non-ring related transmission characteristics.

from the ideal, potentially possible, laser linewidth of <0.003 cm^{-1} (about 0.01 nm at 6 µm), an effective linewidth, that can be mainly attributed to mode-hopping, may reach dimensions of up to 0.1 cm^{-1} (0.4 nm at 6 µm) that limits the experimentally obtainable Q-factor, especially, when attempting to tune the QCL emission wavelength. It is anticipated that devices with stabilized emission intensity or mode-hop-free lasers provide increased Q-factors; hence, it is safe to assume that the Q-factors derived herein are underestimated.

Potential optical scattering losses, *e.g.* due to rough wave-guide sides, or process imperfections, can lead to a reduced experimentally obtainable Q-factor in comparison to the value obtained from the ideal simulation. The rather low Q-factors may be associated with the rather high losses as well as with the decoupling waveguide and indicate apparently efficient decoupling. With the derived values of 0.4 for the roundtrip loss factor α and 0.6 for the field coupling coefficient t, the ring represents an over-coupled case. In this case, light will be coupled back from the ring into the in-coupling waveguide, which leads to a broadened FWHM, *i.e.* a broader bandwidth that is coupled into the ring as for critical coupling case ($\alpha = t$). It was shown that approx. 22% of the detected signal intensity was coupled from the straight waveguide at the resonance wavelength, which is in the range previously calculated (33%) and indicates successful yet improvable decoupling. Since, over-coupling is presumed to be the main reason for the low experimental Q-factor, improved designs for designing the orientation of the de-coupling port, *i.e.* parallel to the in-coupling port or in a pulley like configuration may lead to improved Q-factors in further studies.

In this context, extended optimization of the coupling gap dimensions, *i.e.* width, length (*e.g.* race track designs) and depth (*e.g.* slab-like designs), both theoretically and experimentally, may lead to further improved Q-factors as well as an improved insight into the resonator behaviour.

With optimized micro-ring resonator structures, chem/bio sensing may be achieved by utilizing tunable laser light sources providing sufficient spectral resolution in order to evaluate minute resonance peak shifts within the resonance spectra. In such sensing scenarios, shifts of the wavelength position at resonance arise from analyte exposure of the waveguide changing the effective refractive index (n_{eff}). Consequently, the resonance peak shows an analyte concentration dependent shift. Appropriate surface modification of the waveguide with chem/bio recognition motifs may further enhance analyte interactions in close vicinity of the waveguiding structure, thereby resulting in an even more pronounced refractive index variation yielding an improved analytical sensitivity.

Conclusions

Thin-film micro-ring resonators have been designed, fabricated and were characterized *via* thermal tuning of the resonator structure. The derived Q-factors of the GaAs/AlGaAs rings was approx. 1900.

The limited spectral resolution of the deployed EC-QCL light source was mitigated by the thermal tuning method. In future,

similar studies using light sources with increased spectral resolution such as mode-hop-free (MHF)-QCLs or frequency combs enable further verification of the applied characterization method for evaluating the potential utility of MIR thin-film micro-resonators for chem/bio sensing applications *via* resonant-cavity enhancement and *via* de-multiplexed waveguide structures. In addition, the presented micro-ring resonators are a first step towards even more sophisticated photonic structures based on a GaAs/Al$_{0.2}$Ga$_{0.8}$As waveguide architectures. Further evaluation of the transmission characteristics, chem/bio sensing behaviour, and properties of straight, curved or more complex coupled structures will benefit from the findings provided herein.

Conflicts of interest

There are no conflicts to declare.

Acknowledgements

References

1 R. Soref, *IEEE J. Sel. Top. Quantum Electron.*, 2006, **12**(6), 1678–1687.

2 B. Jalali and S. Fathpour, *J. Lightwave Technol.*, 2006, **24**(12), 4600–4615.

3 M. Li, W. H. P. Pernice, C. Xiong, T. Baehr-Jones, M. Hochberg and H. X. Tang, *Nature*, 2008, **456**(7221), 480–484.

4 A. Yariv, *IEEE Photonics Technol. Lett.*, 2002, **14**(4), 483–485.

5 X. Zheng, I. Shubin, G. Li, T. Pinguet, A. Mekis, J. Yao, H. Thacker, Y. Luo, J. Costa, K. Raj, J. E. Cunningham and A. V. Krishnamoorthy, *Opt. Express*, 2010, **18**(5), 5151.

6 I. Shubin, X. Zheng, G. Li, H. Thacker, J. Yao, B. Guenin, T. Pinguet, A. Mekis, a. V. Krishnamoorthy and J. E. Cunningham, *Proc. SPIE*, 2011, **7944**(11), 794402.

7 D. K. Armani, T. J. Kippenberg, S. M. Spillane and K. J. Vahala, *Nature*, 2003, **421**, 925–928.

8 X. Zhang and A. M. Armani, *Opt. Express*, 2013, **21**(20), 23592–23603.

9 P. Del'Haye, A. Schliesser, O. Arcizet, T. Wilken, R. Holzwarth and T. J. Kippenberg, *Nature*, 2007, **450**(7173), 1214–1217.

10 Y. Sun and X. Fan, *Anal. Bioanal. Chem.*, 2011, **399**(1), 205–211.

11 A. Yalcin, K. C. Popat, J. C. Aldridge, T. A. Desai, J. Hryniewicz, N. Chbouki, B. E. Little, O. King, V. Van, S. Chu, D. Gill, M. Anthes-Washburn, M. S. Unlu and B. B. Goldberg, *IEEE J. Sel. Top. Quantum Electron.*, 2006, **12**(1), 148–155.

12 M. C. Estevez, M. Alvarez and L. M. Lechuga, *Laser Photonics Rev.*, 2012, **6**(4), 463–487.

13 D. Duval and L. M. Lechuga, *IEEE Photonics J.*, 2013, **5**(2), 0700906.

14 A. M. Armani, R. P. Kulkarni, S. E. Fraser, R. C. Flagan and K. J. Vahala, *Science*, 2007, **317**(5839), 783–787.

15 J. Witzens and M. Hochberg, *Opt. Express*, 2011, **19**(8), 7034.

16 X. Wang, M. Sieger and B. Mizaikoff, *Proc. SPIE*, 2013, **8631**, 86312M.

17 M. Sieger and B. Mizaikoff, *Anal. Chem.*, 2016, **88**(11), 5562–5573.

18 B. Mizaikoff, X. Wang, M. Sieger, L. Faraone, J. Antoszewski, W. Lei, M. Jetter and P. Michler, in *2014 Conference on Optoelectronic and Microelectronic Materials & Devices*, IEEE, 2014, pp. 301–302.

19 B. Mizaikoff, *Chem. Soc. Rev.*, 2013, **42**(22), 8683.

20 C. Y. Wong, Z. Cheng, X. Chen, K. Xu, C. K. Y. Fung, Y. Chen and H. K. Tsang, *IEEE Photonic Soc. 24th Annu. Meet. PHO 2011*, 2011, vol. 5, pp. 877–878.

21 C. Y. Wong, Z. Cheng, X. Chen, K. Xu, C. K. Y. Fung, Y. M. Chen and H. K. Tsang, *IEEE Photonics J.*, 2012, **4**(4), 1095–1102.

22 A. Spott, Y. Liu, T. Baehr-Jones, R. Ilic and M. Hochberg, *Appl. Phys. Lett.*, 2010, **97**(21), 213501.

23 Z. Cheng, X. Chen, C. Y. Wong, K. Xu and H. K. Tsang, *IEEE Photonics J.*, 2012, **4**(5), 1510–1519.

24 P. Ma, D.-Y. Choi, Y. Yu, Z. Yang, K. Vu, T. Nguyen, A. Mitchell, B. Luther-Davies and S. Madden, *Opt. Express*, 2015, **23**(15), 19969.

25 S. Radosavljevic, N. T. Beneitez, A. Katumba, M. Muneeb, M. Vanslembrouck, B. Kuyken and G. Roelkens, *Opt. Mater. Express*, 2018, **8**(4), 824.

26 J.-M. Fédéli, P. Labeye, A. Marchant, O. Lartigue, M. Fournier and J.-M. Hartmann, in *Silicon Photonics: From Fundamental Research to Manufacturing*, ed. R. G. Baets, P. O'Brien and L. Vivien, SPIE, 2018, p. 21.

27 T. Schädle and B. Mizaikoff, *Appl. Spectrosc.*, 2016, **70**(10), 1625–1638.

28 C. Charlton, M. Giovannini, J. Faist and B. Mizaikoff, *Anal. Chem.*, 2006, **78**(12), 4224–4227.

29 X. Wang, S.-S. Kim, R. Roßbach, M. Jetter, P. Michler and B. Mizaikoff, *Analyst*, 2012, **137**(10), 2322.

30 J. Haas, R. Stach, M. Sieger, Z. Gashi, M. Godejohann and B. Mizaikoff, *Anal. Methods*, 2016, **8**(36), 6602–6606.

31 M. Sieger, G. Kos, M. Sulyok, M. Godejohann, R. Krska and B. Mizaikoff, *Sci. Rep.*, 2017, **7**, 44028.

32 L. Leidner, M. Ewald, M. Sieger, B. Mizaikoff and G. Gauglitz, *Proc. SPIE*, 2013, **8774**, 87740S.

33 M. Sieger and B. Mizaikoff, *Photonics Res.*, 2016, **4**(3), 106.

34 T. Soma, J. Satoh and H. Matsuo, *Solid State Commun.*, 1982, **42**(12), 889–892.

35 F. G. Della Corte, G. Cocorullo, M. Iodice and I. Rendina, *Appl. Phys. Lett.*, 2000, **77**(11), 1614–1616.